RSC Advances

ROYAL SOCIETY OF CHEMISTRY

www.rsc.org/advances

RSC advances

RSCPublishing

PAPER

Influence of piezoelectric effect on dissolving behavior and stability of ZnO micro/nanowires in solutions

Cite this: DOI: 10.1039/xoxxoooooox

Received ooth January 2012,
Accepted ooth January 2012

DOI: 10.1039/xoxxoooooox

www.rsc.org/

Kui Zhang[a], Junjie Qi[a,*], Yuan Tian[a], Shengnan Lu[a], Qijie Liang[a], Yue Zhang[a,b,*]

We demonstrate the corrosion behavior of ZnO micro/nanowires under stress for the first time. The influence of piezoelectric effect on the corrosion of the ZnO micro/nanowires under acidic and alkaline environment was investigated. The two sides of the bent ZnO micro/nanowires have a significant different corrosion rate while strain-free ZnO micro/nanowires remain the same. The corrosion details of the individual bent ZnO MWs have been observed under various strains estimated from the local curvature model unambiguously. The corrosion phenomena of the bent ZnO MWs in acid and alkaline environment were different. The outer surface of the wire attracts free hydroxide ions and the inner attract hydrogen ions in solutions which promote the chemical reaction due to the effect of the piezoelectric potential generated by strain. The experiment results indicated that corrosion rate is quite sensitive to strain, which provides a reference on the design and evaluation of nanodevices that served in extreme environment.

Introduction

In recent years, ZnO nanomaterials have drawn much attention in the oxide family for numerous applications. A direct band gap of 3.37 ev and large exciton binding energy (60 mev) at room temperature make ZnO a prominent candidate in UV sensor[1, 2].and light emitting diodes. Due to the unique piezoelectric and semiconducting coupled properties, nanogenerators[3] based on nanowires and nanoarrays have been developed. To prevent catastrophic failures people have developed many ways to continuously monitor the state of infrastructure in real time using micro/nanoscale strain sensor[4-8] with highly sensitivity and low-power or even self-powered[7]. Although a lot of progresses have been made on mechanical properties of ZnO micro/nanowires [9-12], few work has been conducted on the force sensor service condition such as acid or alkaline environment. In recent articles, a lot of biosensors based on ZnO nanowires[13-17] were invented owing to its semiconducting, high isoelectric point and high specific surface area. Nanogenerator which was used to harvest energy from the environment such as muscle stretching vibration, biofluid energy complex with biosensors can build self-powered wireless nanosensors for implantable biomedical detections. Despite people have made great efforts on improving the devices performance and investigating the biocompatibility, biosafety and even the biodegradability[18-20] of ZnO materials, there is no report that addresses the strain effects, which can accelerate the reaction in solutions[21] in individual ZnO wire when it is used as biosensor or strain sensor served in body fluid or other solutions.

In this paper, the influence of piezoelectric effect on individual ZnO MWs corrosion behavior has been intensively studied. The strain is induced by bending ZnO MWs, resulting in a continuous variation of strain across each single nanowire. The relationship between the corrosion rate and the strain was obtained. And the strain was estimated by the local curvature with a geometrical model. This study reveals a new principle for coupling chemical and mechanical properties which is helpful for the application of biosensors or strain sensors.

Experimental

The ZnO microwires were synthesized by a common method of chemical vapor deposition, with diameters of 1–10 μm and lengths ranging from several hundred micrometers to several millimeters. Firstly, the mixed ZnO powder and carbon powder with a molar ratio of 1:1 in a mortar were used as the evaporation source. A P-type silicon (Si) wafer with dimension of 8mm×10mm was cleaned by acetone, ethanol and ethyl acetate, respectively. Then, it was coated with a thin film of Au (10 nm) as catalyst layer faced down on a porcelain boat loaded with the mixed power as the source material. Put the boat at the center of the tubefurnace and quickly heated the whole system to 960℃ under a constant flow of 80 sccm Ar, then keep the system at 960℃ for 15 min under a constant flow of 80 sccm Ar mixed with 1 sccm O_2. The Si wafer was air-cooled to room temperature and the white product was collected on the Si wafer consisted of ZnO MWs.

To bend the ZnO MWs under an optical microscope, the ZnO MWs were dispersed onto a cleaned silicon wafer and the wires longer than 1 mm with the diameter about 3 μm were

choosen. The wire was manipulated by a needle tip and the two ends was fixed on Si substrate by silver paste to keep the bend shape[21-27]. Then the silicon wafer was placed in the air for 2 hours to make the sliver paste on the silicon wafer dried completely.

To investigate the corrosion behavior of ZnO MWs under strain, put the bent wires in solution carefully in which the KOH solution concentration of 4 moles per liter and HCl solution (PH≈5.8-6.2) were prepared respectively. Then take out the silicon wafer and clean it out, and dried the samples as soon as possible to reduce the influence of DI water. The morphology of ZnO wires were observed using Field Emission Scanning Electron Microscope(FE-SEM).

Results and discussion

Figure.1(a) shows the SEM image of the synthesized sample with smooth surface. The inset displays a cross-section image of a ZnO wire which appears the hexagonal shape. The bent wire fixed on the Si substrate is displayed in Figure.1(b) and the insert is the high-magnification SEM image of the ZnO wire. The photoluminescence(PL) spectra of the ZnO wires was measured with an He-Cd laser (325 nm) as the excitation source. The room-temperature PL spectra of the nanowires was shown in Figure.1(c), we observed that the UV emission at 380 nm corresponding to the near band-edge emission and a weak green emission intensity at 550 nm, which demonstrated that the prepared ZnO wires have high crystal quality. In order to further characterize the structure of ZnO wires, the room-temperature Raman spectrum of ZnO wires were taken which was illustrated in Figure.1(d). The peaks at 98 cm^{-1},331 cm^{-1}, 438 cm^{-1} and 582 cm^{-1} indicated that the ZnO MWs were a wurtzite hexagonal ZnO structure. Figure.1(e) depicts the XRD pattern of the nanowires. The diffraction peaks can be readily indexed to a hexagonal structure. HRTEM image, low-magnification TEM image of a ZnO wire and the corresponding select-area electron diffraction (SAED) pattern are shown in Figure.1(f), which indicate that the micro/nanowire is a wurtzite structured single crystal, growing along [0001] direction.

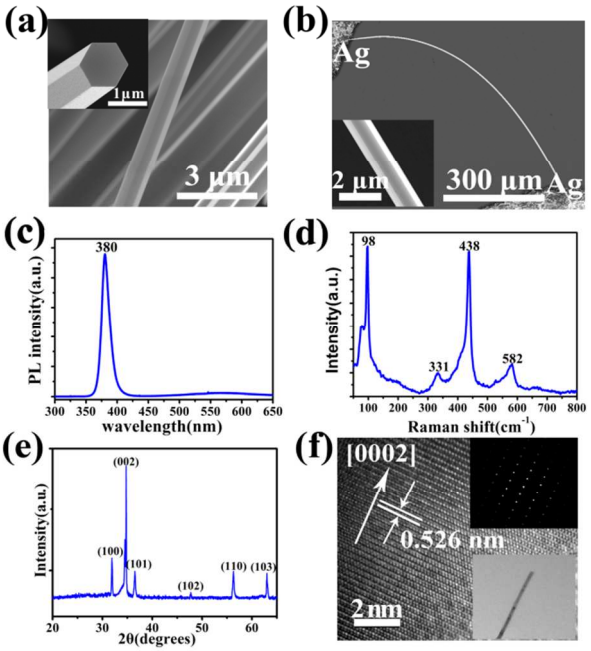

a

Figure.1. (a) SEM image of ZnO MWs grown on the silicon substrate. The inset is a cross-section image of a ZnO wire. (b) SEM image of bent ZnO MW on silicon substrate. (c) Photoluminescence spectrum of the ZnO wires. (d) Raman spectrum of ZnO wires. (e) XRD spectrum of ZnO wires. (f) HRTEM image; the inset is the corresponding low-magnification TEM image and SAED pattern of the ZnO wire.

A strain-free ZnO wire with diameter about 650 nm was prepared on Si wafer, as shown in Figure.2(a). After interacting with 4 M KOH solution for 5, 15, 25 minutes respectively, the morphology of the ZnO wire is exhibited in Figure.2(b-d). The wire becomes coarse and the shape is not regular hexagonal anymore, which can be aggravated by increasing the reaction time. The chemical reaction in this case can be expressed by the equation:

$$ZnO(s)+ 2OH^{-}=ZnO_2^{2-}+H_2O. \quad (1)$$

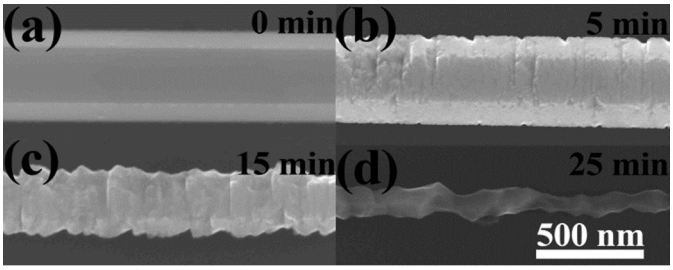

Figure.2. SEM images of an individual ZnO wire that has interacted with 4M KOH solution concentration of for different lengths of time. (a) 0, (b) 5, (c) 15 and (d) 25 minutes, the scale bar in (d) is the same for (a–c).

where ZnO_2^{2-} is soluble. The corrosion behavior of the strain-free ZnO MWs in HCl solution with PH≈5.8-6.2 was also studied. ZnO MWs with diameter of 4 μm (Figure.3a) was chosen to react with HCl solution. The morphologies after different reaction time were shown in Figure.3(b-d), only some pitting corrosion on the surface of the wire was found after 5 minutes. The edge of the wire becomes sharper with the time increased. We can ascribe the etching of the ZnO MWs in HCl solution to the following chemical process:

$$ZnO(s)+ 2H^{+}=Zn^{2+}+H_2O. \quad (2)$$

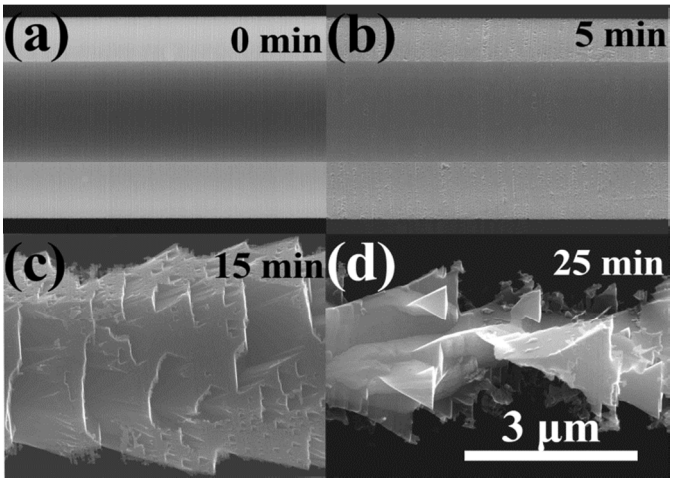

Figure.3. SEM images of a ZnO wire interacted with HCl solution of PH≈5.8-6.2 for different lengths of time. (a) 0, (b) 5, (c) 15 and (d) 25 minutes, the scale bar in (d) is the same for (a–c).

For an ideal curved nanowire, there are enough reasons to deem that the outer(inner) edge of the nanowire endure a

tensile(compressive) strain, while the middle of the nanowire is free of any strain, as depicted in Figure.4(a, b).

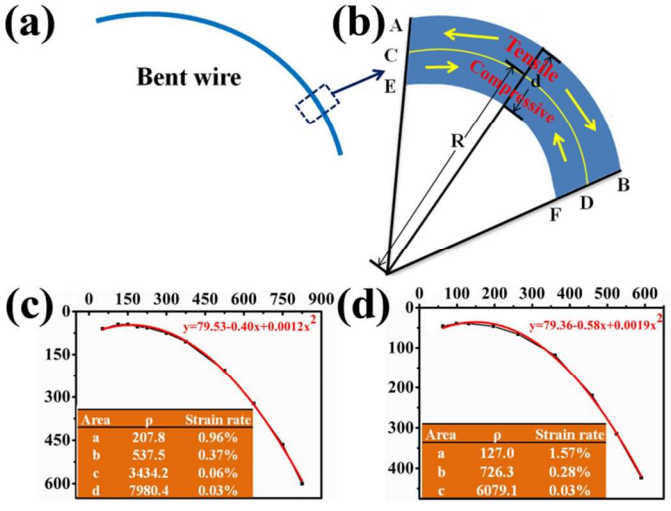

Figure.4. (a) and (b) Schematic plot of a bent ZnO wire to estimate the strain rate from measuring the local curve radius of the wire. (c) and (d) Simulation curve of the bent ZnO wires to estimate the areas strain rate.

In order to get the strain rate of different areas, a geometric model shown in Figure.4(b) was used. The strain rate(ε) can be calculated using the local curvature radius (ρ) and the diameter d of the wires.[26]

$$\varepsilon=(\widehat{AB}-\widehat{CD})/\widehat{CD}=d/2R \qquad (3)$$

Where R is the local curvature radius. In this paper, two different bent MWs were prepared. We put the bent wires of Figure.5(A) and Figure.6(A) in a two-dimensional coordinate system and ten points on the wires have been taken out to fit out the curves equation on the basis of the shape, as shown in Figure 4(c, d):

$$y=79.53-0.40x+0.0012x^2 \qquad (4)$$

$$y=79.36-0.58x+0.0019x^2 \qquad (5)$$

where x is the horizontal ordinate and y is the vertical coordinate.

According to the above equation we can measure the local curvature radius (ρ) of the wire with the formula:

$$\rho = \left|\frac{\left(1+y'^2\right)^{\frac{3}{2}}}{y''}\right| \qquad (6)$$

y' is first derivative and y" is second derivative. The inset of Figure.4(c-d) show the corresponding ρ of the rectangular areas in Figure.5(A) and Figure.6(A).

In order to observe the influence of the strain effect on corrosion behavior of ZnO wire, a bent wire with diameter about 3.8 μm and length about 1 mm was prepared in Figure.5(A) and the insert is a high-magnification SEM image. The strain rate of ZnO wire in different rectangular areas of 'a-d' are 0.96%, 0.37%, 0.06%, 0.03%, respectively. Figure.5(B) display the high-magnification SEM images of the different regions in (A) interact with KOH solution for 5, 15, 25, 35 minutes respectively, When the etching time reach to 35 mins the rectangular area of 'a'(Figure.5(A)) cracked. The diameter of the ZnO wire decreased faster in KOH solution when the wire suffered a larger strain, and the outer of the wire surfaces corrodes more rough and irregular than that of the inner sides of the wire and this become even more serious when the strain increases.

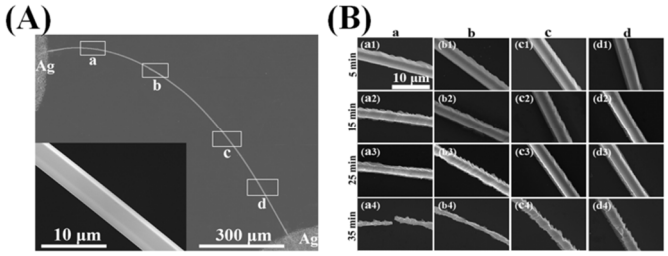

Figure.5. SEM images of a bent ZnO wire interacted with KOH solution concentration of 4M for different lengths of time. (A) Low-magnification SEM image of the ZnO wire. (B) High-magnification SEM image of the different regions in (A) interact with KOH solution for 5, 15, 25, 35minutes respectively, (a1-a4) area **a**, (b1-b4) area **b,** (c1-c4) area **c,** (d1-d4) area **d.** The scale bar in (a1) is the same for all the left.

To attest the phenomenon, we designed another experiment. Figure.6(A) shows a Low-magnification SEM image of the bent ZnO wire about 0.8 mm long with diameter about 1.65 μm, and the high-magnification SEM image of the rectangular areas in inset of Figure.6(A) which was corroded by HCl solution for different time are shown in Figure.6(B). When the etching time reach to 25 mins the rectangular area of 'a'(Figure.6(A)) cracked. The corrosion behavior is similar with that of in KOH solution except the inner of the wire surfaces corrodes more rough and irregular than that of the outer sides.

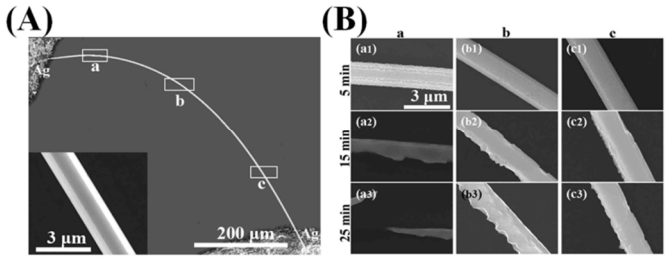

Figure.6. SEM images of a bent ZnO wire interacted with HCl solution of PH≈6 for different lengths of time. (A) Low-magnification SEM image of the ZnO wire. (B) High-magnification SEM image of the different regions in (A) interact with HCl solution for 5, 15, 25 minutes respectively, (a1-a3) area a, (b1-b3) area b, (c1-c3) area c. The scale bar in (a1) is the same for all the left.

The diameters reduction rate of the two bent wires with different strain rate and the reaction time is presented in Figure.7(a-b). The diameter of ZnO wires decrease with the increasing of Etching time, and the diameter change is more pronounced when the wire is under a higher strain. The diameter change behavior of ZnO wires follow the same law in the two solutions.

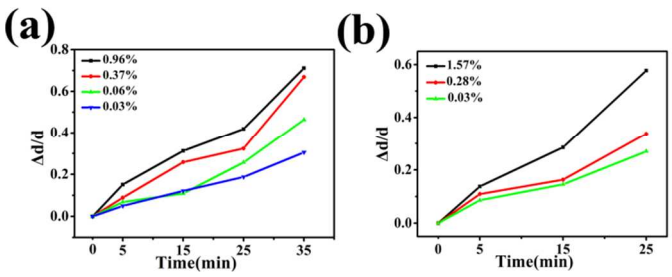

Figure.7. The diameter reduction rate of the two bent wires in corresponding to different regions in Figure.5 and Figure.6 in different solution (a) KOH (b) HCl

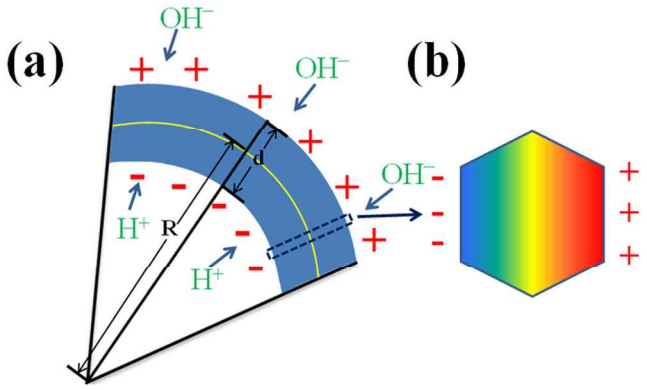

Figure.8. (a) piezoelectric effects of inner and outer of the wire which attract hydrogen ion and hydroxyl ion. (b) Cross-sectional Schematic diagrams of bending induced piezoelectric effects. The rain bow color stands for the potential distribution in the wire induced by bending.

ZnO wire produces the piezoelectric effects when it is suffered strain[3, 28, 29], Positive(negative) chargers were generated on the outer (inner) side of the wire surface which vanished only when the strain was released, as depicted in Figure.8(a). Piezoelectric effect accelerates the corrosion rate of ZnO wires in solutions. The outer surface of the wire attracts free hydroxide ions and the inner attract hydrogen ions in solutions which can promote the chemical reaction. In addition, the lattice constant along the c-axis of the bent wire changed, the outer surface of the wire become larger while the inner of the wire get smaller, which accelerates the chemical reaction.

Conclusions

In conclusion, we lay emphasis on the study of the piezoelectric effect on corrosion behavior of ZnO wire in acidic and alkaline environment. We chose KOH solution and HCl solution as the simulated environment. The strain-free ZnO wire corroded almost symmetrically in solutions, while the bent wire corroded quite differently and the failure phenomenon appears faster under a larger strain due to a higher piezoelectric potential. This may reminder the afterward investigators considering the phenomenon when ZnO-based devices were used in biosensor, strain sensor and so on. To the authors' knowledge, this is the first report on the observation of stress corrosion in ZnO nanowires and this will inspired the research of stress corrosion in piezoelectric materials.

Acknowledgements

This work was supported by the National Major Research Program of China (2013CB932600), the Program of International S&T Cooperation (2012DFA50990), NSFC (51232001, 51172022), the Research Fund of Co-construction Program from Beijing Municipal Commission of Education, the Fundamental Research Funds for the Central Universities, Program for Changjiang Scholars and Innovative Research Team in University.

Notes and references

[a] School of Materials Scinece and Engineering, University of Science and Technology Beijing, Beijing 100083, People's Republic of China

[b] Key Laboratory of New Energy Materials and Technologies, University of Science and Technology Beijing, Beijing 100083, People's Republic of China

*Corresponding authors: junjieqi@ustb.edu.cn; yuezhang@ustb.edu.cn

1. D. Gedamu, I. Paulowicz, S. Kaps, O. Lupan, S. Wille, G. Haidarschin, Y. K. Mishra and R. Adelung, *Adv Mater*, 2014, **26**, 1541-1550.
2. J. Qi, X. Hu, Z. Wang, X. Li, W. Liu and Y. Zhang, *Nanoscale*, 2014.
3. Y. Gao and Z. L. Wang, *Nano letters*, 2007, **7**, 2499-2505.
4. Q. Liao, M. Mohr, X. Zhang, Z. Zhang, Y. Zhang and H. J. Fecht, *Nanoscale*, 2013, **5**, 12350-12355.
5. S. Lu, J. Qi, Z. Wang, P. Lin, S. Liu and Y. Zhang, *RSC Advances*, 2013, **3**, 19375.
6. I. Shakir, Z. Ali, J. Bae, J. Park and D. J. Kang, *RSC Advances*, 2014, **4**, 6324.
7. Z. Wang, J. Qi, X. Yan, Q. Zhang, Q. Wang, S. Lu, P. Lin, Q. Liao, Z. Zhang and Y. Zhang, *RSC Advances*, 2013, **3**, 17011.
8. H. Gullapalli, V. S. Vemuru, A. Kumar, A. Botello-Mendez, R. Vajtai, M. Terrones, S. Nagarajaiah and P. M. Ajayan, *Small*, 2010, **6**, 1641-1646.
9. P. Li, Q. Liao, S. Yang, X. Bai, Y. Huang, X. Yan, Z. Zhang, S. Liu, P. Lin, Z. Kang and Y. Zhang, *Nano letters*, 2014, **14**, 480-485.
10. R. Agrawal, B. Peng and H. D. Espinosa, *Nano letters*, 2009, **9**, 4177-4183.
11. F. Xu, Q. Qin, A. Mishra, Y. Gu and Y. Zhu, *Nano Research*, 2010, **3**, 271-280.
12. A. Asthana, K. Momeni, A. Prasad, Y. K. Yap and R. S. Yassar, *Nanotechnology*, 2011, **22**, 265712.
13. R. Yu, C. Pan, J. Chen, G. Zhu and Z. L. Wang, *Advanced Functional Materials*, 2013, **23**, 5868-5874.
14. F. Patolsky, G. Zheng and C. M. Lieber, *Analytical Chemistry*, 2006, **78**, 4260-4269.
15. J. M. Moon, Y. Hui Kim and Y. Cho, *Biosensors & bioelectronics*, 2014, **57**, 157-161.
16. R. Yakimova, L. Selegård, V. Khranovskyy, R. Pearce, A. Lloyd Spetz and K. Uvdal, *Frontiers in bioscience (Elite edition)*, 2012, **4**, 254-278.
17. Y. Zhao, X. Yan, Z. Kang, P. Lin, X. Fang, Y. Lei, S. Ma and Y. Zhang, *Microchimica Acta*, 2013, **180**, 759-766.
18. J. Zhou, N. S. Xu and Z. L. Wang, *Advanced Materials*, 2006, **18**, 2432-2435.
19. W. Zhou, X. Dai, T. M. Fu, C. Xie, J. Liu and C. M. Lieber, *Nano letters*, 2014, **14**, 1614-1619.
20. Z. Li, R. Yang, M. Yu, F. Bai, C. Li and Z. L. Wang, *The Journal of Physical Chemistry C*, 2008, **112**, 20114-20117.
21. S. Xu, W. Guo, S. Du, M. M. Loy and N. Wang, *Nano letters*, 2012, **12**, 5802-5807.
22. X. Han, L. Kou, Z. Zhang, Z. Zhang, X. Zhu, J. Xu, Z. Liao, W. Guo and D. Yu, *Adv Mater*, 2012, **24**, 4707-4711.
23. X. Han, L. Kou, X. Lang, J. Xia, N. Wang, R. Qin, J. Lu, J. Xu, Z. Liao, X. Zhang, X. Shan, X. Song, J. Gao, W. Guo and D. Yu, *Advanced Materials*, 2009, **21**, 4937-4941.
24. C. P. Dietrich, M. Lange, F. J. Klüpfel, H. von Wenckstern, R. Schmidt-Grund and M. Grundmann, *Applied Physics Letters*, 2011, **98**, 031105.
25. J. Chen, G. Conache, M. E. Pistol, S. M. Gray, M. T. Borgstrom, H. Xu, H. Q. Xu, L. Samuelson and U. Hakanson, *Nano letters*, 2010, **10**, 1280-1286.
26. H. Xue, N. Pan, M. Li, Y. Wu, X. Wang and J. G. Hou, *Nanotechnology*, 2010, **21**, 215701.
27. Z. M. Liao, H. C. Wu, Q. Fu, X. Fu, X. Zhu, J. Xu, I. V. Shvets, Z. Zhang, W. Guo, Y. Leprince-Wang, Q. Zhao, X. Wu and D. P. Yu, *Scientific reports*, 2012, **2**, 452.
28. Z. L. Wang, *Advanced Materials*, 2007, **19**, 889-892.
29. S. Yang, L. Wang, X. Tian, Z. Xu, W. Wang, X. Bai and E. Wang, *Advanced Materials*, 2012, **24**, 4676-4682.